A Terminal Hydride Complex of High-spin Mn

Alex Drena,[2]† Addison Fraker,[1]† Niklas B. Thompson,[3] Peter E. Doan,[2] Brian M. Hoffman,[2]* Alex McSkimming,[1]**

[1]Department of Chemistry, Tulane University, New Orleans, LA 70118; [2]Department of Chemistry, Northwestern University, Evanston, IL 60208; [3]Chemical Sciences and Engineering Division, Argonne National Laboratory, Lemont, IL 60439.

*bmh@northwestern.edu

**amcskimming@tulane.edu

† Signifies equal contributions.

ABSTRACT

The iron-molybdenum cofactor of nitrogenase (FeMoco) catalyzes fixation of N_2 via Fe hydride intermediates. Our understanding of these species has relied heavily on the characterization of well-defined 3d metal hydride complexes, which serve as putative spectroscopic models. Although the Fe ions in FeMoco, a weak-field cluster, are expected to adopt locally high-spin $Fe^{2+/3+}$ configurations, synthetically-accessible hydride complexes featuring d^5 or d^6 electron counts are almost exclusively low-spin. We report herein the isolation of a terminal hydride complex of four-coordinate, high-spin (d^5; $S = 5/2$) Mn^{2+}. EPR and ENDOR studies reveal an unusually large degree of spin density on the hydrido ligand. In light of the isoelectronic relationship between Mn^{2+} and Fe^{3+}, our results are expected to inform our understanding of the valence electronic structures of reactive hydride intermediates derived from FeMoco.

INTRODUCTION

Transition metal hydride complexes are ubiquitous throughout synthetic inorganic[1,2] and bioinorganic[3-7] chemistry. With respect to the latter, we have maintained a longstanding interest in the Fe–Mo cofactor (FeMoco) of nitrogenase enzymes. This elaborate [Fe_7S_9MoC] metallocluster catalyzes the reduction of atmospheric N_2 to bioavailable NH_3 as part of the global nitrogen cycle,[8] and in doing so supports roughly half the world's human population.[9] To bind and activate the highly inert N_2, FeMoco must first, during turnover, be 'primed' via the accumulation of 4 H^+ and

4 e^- to afford the so-called $E_4(4H)$, or 'Janus' intermediate (Figure 1).[10] A paradigm shift in our understanding of FeMoco came with the recognition that $E_4(4H)$ contains two chemically equivalent Fe hydrides,[11] whose reductive elimination to H_2 drives coordination of N_2 to one or more Fe site(s).[12]

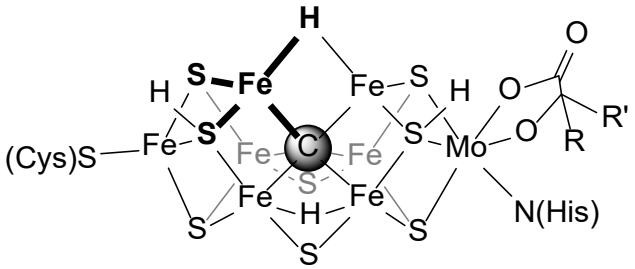

Figure 1. One (of many) possible structures for the $E_4(4H)$ intermediate of FeMoco.

EPR and ENDOR spectroscopies have been central in identifying and characterizing the $S = 1/2$ $E_4(4H)$ state,[10-14] as well as other FeMoco intermediates featuring Fe–H bonds.[15] In this process, structural and electronic assignments have relied heavily on comparisons to synthetic analogues,[16-21] the majority of which feature strong-field supporting ligands and are, as a result, low-spin.[16-18, 20-21] Useful as these model complexes have been, FeMoco is a relatively weak-field cluster, and, as such, transition metal hydrides that adopt locally high-spin configurations are more faithful spectroscopic models. Metal hydrides that model the low-coordinate (≤5), weak-field Fe sites within FeMoco are not uncommon.[19, 22-45] Within this group, however, only a handful bear the half-integer spin required for meaningful ENDOR analysis, let alone the d^5 or d^6 configurations expected for Fe^{2+} and Fe^{3+}, respectively.[19]

FeS clusters, including FeMoco,[46] have long been known to feature highly delocalized electronic structures.[47] For example, cuboidal $[Fe_4S_4]^{2+}$ clusters, which consist of (formally) two locally high-spin Fe^{2+} and two locally high-spin Fe^{3+} centers, are typically best described as $[Fe^{2.5+}{}_4S_4]^{2+}$, i.e. completely valence delocalized. Recently, however, it has been shown that certain strong-field ligands are able to disrupt electron exchange in such clusters, resulting in valence localization.[48-52] Most pertinently, a single akyl ligand causes the bound Fe center to adopt partial,[48] or indeed strong,[49] Fe^{3+} character. Given the similar donor properties between alkyl and hydrido ligands, it seems possible that Fe–H sites in any FeMoco intermediates might be valence localized, most plausibly as Fe^{3+}. We have consequently been drawn to the chemistry of terminal, high-spin Mn^{2+} hydrides, which are isoelectronic to high-spin Fe^{3+} hydrides, but considerably less

oxidizing and so, presumably, more stable. Although a number of Mn hydrides have been reported, only the polynuclear $\{[^{tBu3}CpMn]_4[MnH_6]\}$[53] and the recently reported[54] $[(dmpe)_2MnH(L)]^+$ are open-shell; both are low-spin (S = 1/2) at the hydride-bound Mn.

Our lab has recently developed a new class of N,N,C heteroscorpionates (^{R}**L**; where R denotes the metal-adjacent pyrazolyl substituents, Scheme 1))[55-56] inspired by the 'weak-weak-strong'-field donor environment of the Fe sites in FeMoco (c.f. Figure 1). We postulated such ligands would be well-suited to support terminal, 3d metal hydrides due to a i) large, readily modulated steric profile able to hinder dimerization[27-30, 33-37, 41, 44-45] and ii) high σ-donicity, which should act to suppress reductive elimination of H_2 or ^{R}**L**H. We report herein the synthesis and characterization of a terminal hydride complex of high-spin (S = 5/2) Mn^{2+}, (^{tBu}**L**)MnH. Q-band EPR measurements show that this complex exists in a novel zero-field splitting regime, while ^{1,2}H ENDOR reveals that spin-density on the hydride is substantially greater than for any other previously reported synthetic complex. Our results provide a potentially valuable point of reference for the continued elucidation of the electronic structure of hydride-bound FeMoco states.

RESULTS

Synthesis and Characterization

As per our established procedures,[55-56] deprotonation of ^{tBu}**L**H followed by metalation with $MnI_2(THF)_3$ gave the corresponding high-spin Mn^{2+} complex (^{tBu}**L**)MnI as a pale yellow, crystalline solid in ~64% yield (Scheme 1). Addition of 1.5 equivs. $K[Et_3BH]$ to (^{tBu}**L**)MnI resulted in an appreciable darkening of the reaction solution, from which the terminal hydride complex (^{tBu}**L**)MnH could be isolated (38% yield; see SI). (^{tBu}**L**)MnI and (^{tBu}**L**)MnH have very similar ^{1}H

Scheme 1. Synthesis of (^{tBu}**L**)MnH and its deuterium labelled congener. Ar^F = 3,5-$(CF_3)C_6H_3$.

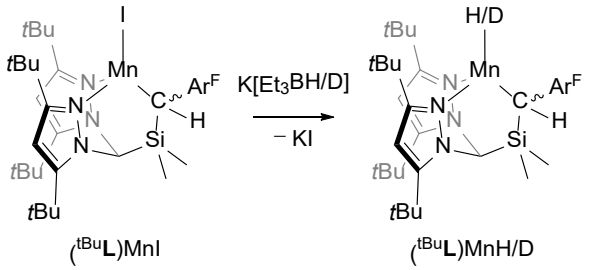

NMR spectra and solution state magnetic moments of 6.1 and 6.0 μ_B, respectively, suggesting a high-spin state at Mn for both with only minimal orbital contributions. We similarly prepared the deuterium labelled complex (^{tBu}**L**)MnD from (^{tBu}**L**)MnI and K[Et_3BD]; the latter reagent was prepared via a new methodology employing cheap and widely available LiD (see SI), which we anticipate others will find broadly useful in the synthesis of other deuteride complexes.

The structures of (^{tBu}**L**)MnI and (^{tBu}**L**)MnH were determined by single crystal X-ray diffraction (XRD) methods; (^{tBu}**L**)MnH is shown in Figure 2. The Mn–^{tBu}**L** donor distances are very similar in both complexes and are typical for high-spin Mn^{2+}; for example, d(Mn–C_{alkyl}) = 2.178(2) and 2.215(1) Å for (^{tBu}**L**)MnI and (^{tBu}**L**)MnH, respectively. The hydrido ligand for (^{tBu}**L**)MnH was located in the difference map and its location freely refined. The determined position renders the Mn center pseudo-threefold symmetric about the Mn–H bond, i.e. $\angle$ C_{alkyl}–Mn–H ≈ $\angle N_{pz1}$–Mn–H ≈ $\angle N_{pz2}$–Mn–H ≈ 120° with τ_4 = 0.79. Although care should be taken in interpreting M–H distances without neutron diffraction data, we note that the XRD determined Mn–H bond length of 1.68(2) Å is similar to that obtained for high-spin, four-coordinate terminal hydride complexes of Co and Fe,[19, 22-23, 26, 43] and is in good agreement with our calculations (see SI). A weak resonance at 1506 cm^{-1} in the FTIR spectrum of (^{tBu}**L**)MnH was identified as the Mn–H stretch, which is red shifted by the expected factor of 1.4 in (^{tBu}**L**)MnD. The computed value of 1588 cm^{-1} is somewhat higher, but in reasonable agreement. (^{tBu}**L**)MnH appears, then, to feature

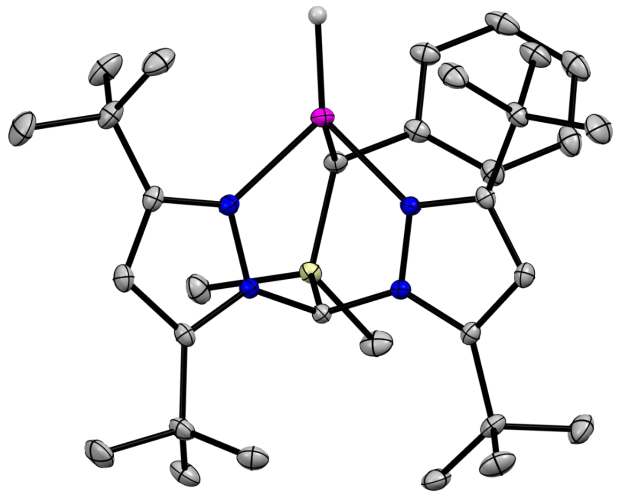

Figure 2. Thermal ellipsoid plot (50%) of (^{tBu}**L**)MnH. Pink, blue, yellow, and gray ellipsoids represent Mn, N, Si, and C, respectively. Hydrogen atoms except that bound to Mn, solvent molecules and CF_3 groups are omitted for clarity.

a remarkably, if predictably, weaker Mn–H bond c.f. reported low-spin Mn terminal hydrides (e.g. for $[(dmpe)_2MnH(L)]^+$, ν(Mn-H) > 1700 cm^{-1}).[54, 57] A similar observation has been noted, for example, for the high-spin (S = 1) TpCoH ν(Co-H) = 1669 cm^{-1}.[22]

EPR Spectroscopy

Figure 3a shows 35 GHz absorption-display EPR spectra of (^{tBu}**L**)MnH, (^{tBu}**L**)MnD and (^{tBu}**L**)MnI obtained by rapid-passage, CW EPR at 2 K. As expected, the highly articulated spectra of (^{tBu}**L**)MnH and (^{tBu}**L**)MnD are essentially the same, while that of (^{tBu}**L**)MnI differs significantly. Figure 3b compares the experimentally derived 2 K EPR spectrum for (^{tBu}**L**)MnH (black trace) and a simulation obtained using EasySpin[58] (red trace). Despite the presence of substantial structure in the (^{tBu}**L**)MnH/D spectra, they could be simulated well with a small range of zero field splitting (ZFS) parameters. The set of parameters was then optimized by the requirement that both EPR and H/D ENDOR spectra be well simulated, as described below.. The simulations shown in Figure 3b employed ZFS parameters D = 7,600 MHz (0.25 cm^{-1}), E/D = 0.15; in terms of a general ZFS tensor, these parameters are $D = (3/2)D_z$, $E = ½(D_x – D_y)$. In addition, the g-tensor is assumed isotropic, g = 2.0, as the typically spherical spin distribution of the ground S-state of high-spin Mn^{2+} quenches orbital angular momentum, resulting in negligible g-anisotropy. Although Mn hyperfine is not resolved, use of a 'standard' isotropic hyperfine value $a_{iso}(^{55}Mn)$ = −250 MHz optimized the simulation. (^{tBu}**L**)MnI exhibits a much larger ZFS (D = 24,000 MHz (0.83 cm^{-1})) than that of (^{tBu}**L**)MnH (Figure S17). The sensitivity of the ZFS in mononuclear Mn^{2+} ions to their ligand environment is well-established,[59-61] with drastic differences even within the halide series.[62] In fact, the parameters for (^{tBu}**L**)MnI agree well with those previously reported for iodide complexes, though it is worth noting that this is the first Mn^{2+} complex with a single iodide ligand so studied.[62-66]

As illustrated in Figure 3b, the spectrum obtained for (^{tBu}**L**)MnH is the sum of contributions from the five EPR-allowed transitions ($m_s \rightarrow m_s + 1$) between electron-spin sublevels ($-5/2 \leq m_s \leq 3/2$), with intensities of the contributions decreasing with increasing m_s due to Boltzmann depopulation at 2 K. The breadth and shape of the observed spectra are dominated, respectively, by the axial (D) and rhombic (E) ZFS parameters. The five EPR-allowed transitions include a roughly-isotropic, central $-1/2 \rightarrow +1/2$ transition and the four highly anisotropic satellite

transitions, which give highly orientation-selective ENDOR responses.[67] Of particular importance for the ENDOR measurements discussed below, the EPR intensity at the low-field edge of the observed spectrum (~5 kG ↔ ~ 7 kG) is dominated by the contribution from the –5/2 → –3/2 manifold. For *D, E* > 0 this edge of this manifold predominantly arises from 'single-crystal-like' orientations in which the *Y*-axis of the ZFS tensor is aligned with the external magnetic field,[67-68]

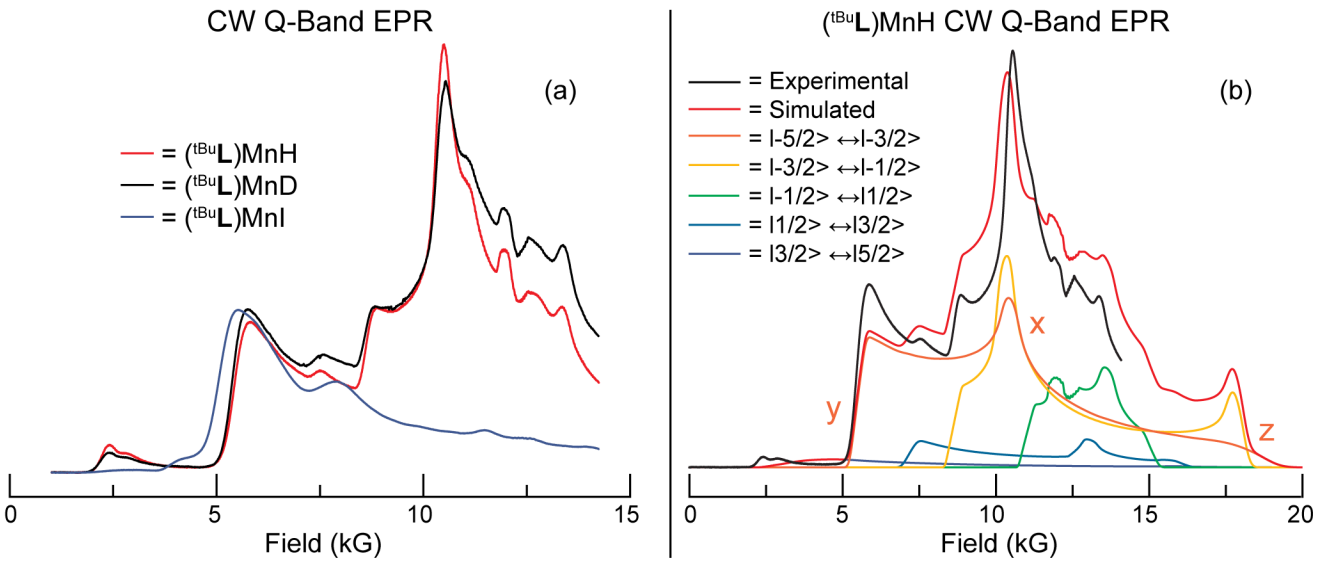

Figure 3. (a) 2 K 35 GHz absorption-display CW EPR spectra of (^{tBu}**L**)MnH (red trace), (^{tBu}**L**)MnD (black trace), and (^{tBu}**L**)MnI (blue trace). Microwave frequency: 34.874 GHz (-H), 34.934 GHz (-D), 34.923 GHz (-I); power attenuation: 20 dB; modulation: 1.6 G; time constant: 64 ms. Spectra scaled arbitrarily for clarity. (b) Absorption-display EPR of (^{tBu}**L**)Mn(H) (black trace) with simulation (red trace) and the contributions from individual transitions differentiated by color. ZFS principal axes are labeled for the –5/2 → –3/2 manifold. The high field edge of the experimental spectrum is limited by the available magnetic fields. Parameters used for simulation are D = 7,600 MHz (0.25 cm^{-1}; E/D = 0.15; A = 250 MHz; f = 0.05, g = 2.0.

and so a set of related orientations are interrogated in the ~5 kG – 7 kG range. In the higher magnetic field range of ~11 kG ↔ 15 kG the EPR spectrum has significant contributions from the m_s = –5/2 and –3/2 satellite manifolds and the central –1/2 → +1/2 transition. ENDOR spectra collected in both field ranges are reported below.

Single-Crystal-Like ENDOR spectra along D_Y of (^{tBu}L)MnH/D EPR Envelope. As thus noted, low temperature ENDOR at the low field edge of the EPR envelope selectively probes the –5/2 → –3/2 transition manifold and yields single-crystal-like ENDOR spectra for molecules oriented so that the external field lies along the *Y*-axis of the ZFS *D*-tensor.[67-68] A ^{1}H Davies ENDOR spectrum thus collected, Figure 4a, shows two sharp peaks at 23 MHz and 62 MHz for (^{tBu}**L**)MnH (red trace) that are absent in (^{tBu}**L**)MnD (black trace); these can be interpreted as

corresponding to a ^{1}H doublet with an *effective/observed* hyperfine coupling constant of $A' = -39$ MHz, whose magnitude differs from the intrinsic spin-Hamiltonian parameter, as treated below, and in greater detail in the SI. In addition, the procedure for determining the sign of the coupling is presented in the SI. This effective value for this hydride coupling is confirmed by the ^{2}H Davies ENDOR spectrum of (^{tBu}**L**)MnD in Figure 4b, which shows a corresponding doublet at 3.5 MHz

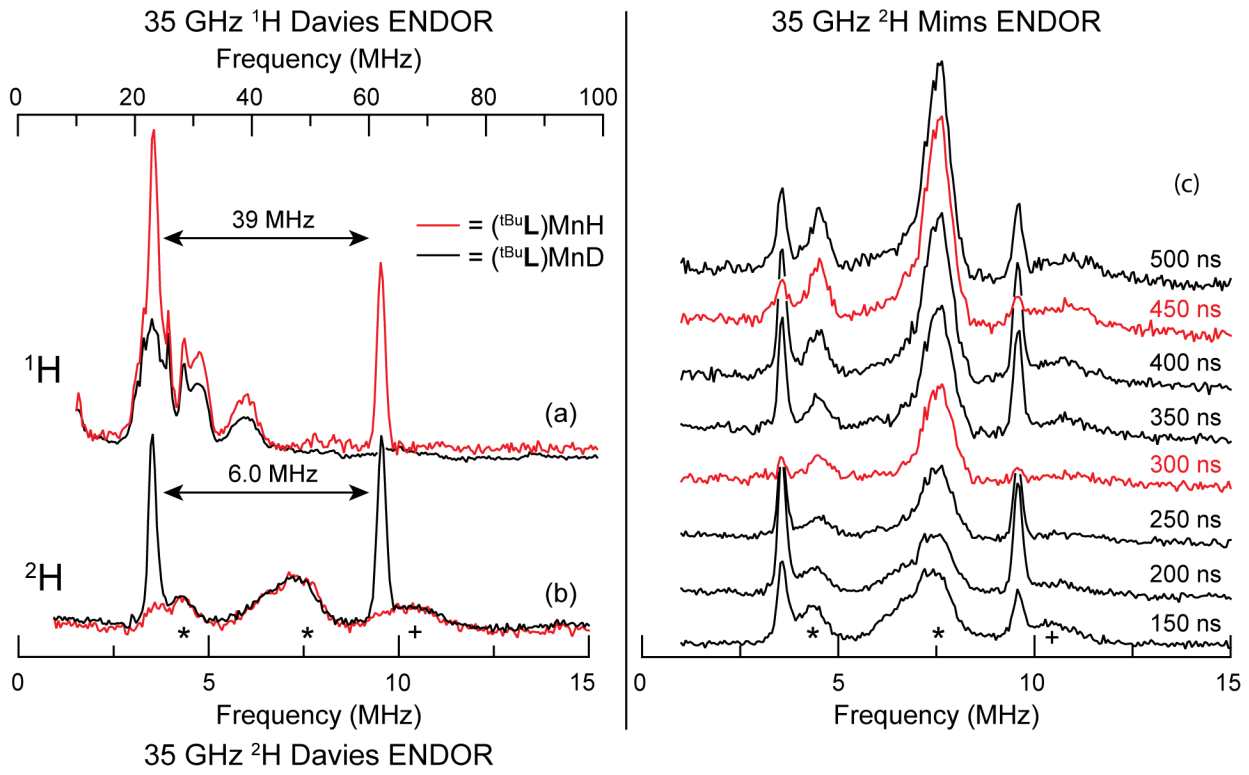

Figure 4. (a) ^{1}H and (b) ^{2}H Davies ENDOR for (^{tBu}**L**)MnH (red trace) and (^{tBu}**L**)MnD (black trace) at 5.35 kG and 2 K. Appearance of the frequency axis in (b) is scaled by a factor of 6.5 to account for the difference in g_n between ^{1}H and ^{2}H. Microwave frequency: 34.6 GHz; microwave pulse length (π): 80 ns (^{1}H Davies), 200 ns (^{2}H Davies); τ: 600 ns; RF pulse length: 15 µs (^{1}H Davies), 60 µs (^{2}H Davies); repetition rate: 5 ms. Spectra intensities have been scaled arbitrarily for clarity. (c) 35 GHz ReMims ENDOR of (^{tBu}**L**)MnD at 5.35 kG and 2 K. Spectra exhibiting Mims suppression effect are shown in red. Microwave frequency: 34.6 GHz; microwave pulse length ($\pi/2$): 30 ns; τ_1: varied from 150 – 500 ns as shown in figure; τ_2: τ_1 + 200 ns; RF pulse length: 60 µs; repetition rate: 5 ms. Spectra scaled to the relative intensity of their observed echo height. 3rd and 5th proton harmonic (*); ^{14}N background signal (+).

and 9.5 MHz that is absent in the spectrum for (^{tBu}**L**)MnH (red trace), and whose frequency difference yields a matching effective constant of $A' = -6.0$ MHz, as predicted by the ratio of ^{1}H and ^{2}H nuclear g-values [$g_n(^{1}\mathrm{H})/g_n(^{2}\mathrm{H}) = 6.5 = A'_s(^{1}\mathrm{H})/A'(^{2}\mathrm{H})$]. Note the absence of quadrupole splitting of the narrow ^{2}H peaks, as is to be expected for a hydride ion with roughly double-occupancy of its 1*s* orbital involved in a polar σ bond with Mn.

The assignment of the two ^{2}H peaks as a –5/2 → –3/2 hyperfine-split doublet with an effective splitting of A' = –6.0 MHz is verified by the τ dependence of the ReMims (see Experimental, SI) ENDOR response (Figure 4c). ReMims ENDOR follows the same τ-dependence of the signal as Mims ENDOR, with "blind spots" (ENDOR nulls) when A (MHz)•τ (μs) = n, n = 0,1,2,....[69] Mims ENDOR is limited by the deadtime of the experiment, while ReMims circumvents this by use of a four-pulse stimulated echo detection subsequence, allowing for the use of much shorter τ values.[70-71] The resulting suppression of the observed doublet in Figure 4c (red traces) at τ = 300 and 450 ns corresponds to the measured effective hyperfine A' = –6 MHz for n = 2 and 3, establishing that these peaks are indeed a doublet separated by this effective hyperfine coupling constant.

The *observed* hyperfine coupling differs from the *intrinsic* coupling because of an 'intermediate' magnitude of the ZFS term for (^{tBu}**L**)MnH compared to the electron Zeeman at Q-band, neither much smaller nor much larger, which causes significant mixing of m_s substates. This 'intermediate' regime can, of course, be treated by exact calculations such as those performed for simulation with EasySpin, and such simulations are indeed done below. However, the m_s mixing phenomenon is sufficiently unusual that it is appropriate to illuminate it with a perturbation-theory approach involving first-order modifications to the electron spin m_s subfunctions by the ZFS interaction. The resultant frequencies for ENDOR transitions involving the two, *corrected*, lowest-energy electron-spin states when the external field lies along the Y direction of the ZFS tensor (low-field edge of the EPR spectrum) can be written in terms of an m_s formalism (see eqs. S1) by incorporating a correction factor, Δ, that accounts for the axial and rhombic contributions of the ZFS term to mixing of the true m_s substates (eqs. 1, 2). As a result, the observed/effective hyperfine splitting along the Y-axis of the ZFS tensor, now specified as A_Y' and defined as the difference in frequencies of the ENDOR doublet, $\Delta\nu^{obs}$, is related to the intrinsic hyperfine constant along the Y-axis, denoted A_Y, and Δ, through eqs 1, 2.

$$|A_Y'| \equiv \Delta\nu^{obs} = |A_Y(1 + 14\Delta^2)| \qquad \textbf{(1)}$$

$$\Delta = \frac{\epsilon}{4\beta_e \mathrm{B}} \qquad \epsilon = \tfrac{1}{2}(D_{xx} - D_{zz}) \qquad \textbf{(2)}$$

This treatment is explained in detail in the SI. The observed splitting for (^{tBu}**L**)MnH, A_Y' = –6.0 MHz, combined with the ZFS parameters determined by the above EPR simulation, gives an

intrinsic hyperfine constant $A_Y = -5.2$ MHz, which is supported by the exact simulations presented in the following section.

Determination of the full ^{1,2}H Hyperfine Tensor through analysis of 2D field-frequency patterns of 2H ENDOR spectra. In contrast to other studies of paramagnetic metal hydrides,[16-21] the complexity of the EPR spectrum of the $S = 5/2$ (^{tBu}**L**)MnH/D complexes (Figure 3) makes it impracticable to collect and analyze a full 2-D ENDOR pattern. However, by collecting spectra over two field ranges, one spanning fields dominated by the lowest-lying –5/2 → –3/2 manifold, now discussed, and a second spanning fields near $g = 2$ (~12.5 kG at Q-Band), discussed next, and analyzing both patterns through exact simulations (i.e. through full matrix diagonalization) using EasySpin, the full ^{1,2}H hyperfine tensor has been determined.

ENDOR spectra at fields across the low-field edge of the EPR spectrum. Orientation-selective ENDOR spectra of the 2-D pattern of (^{tBu}**L**)MnD, collected from 5.35–7.15 kG (Figure 5), show broadening and splitting due to hyperfine anisotropy of the sharp doublet seen at the lowest field. Superimposed on the experimental spectra are EasySpin simulations (in red) calculated with the parameters for the electron-spin Hamiltonian described in Figure 3b and using

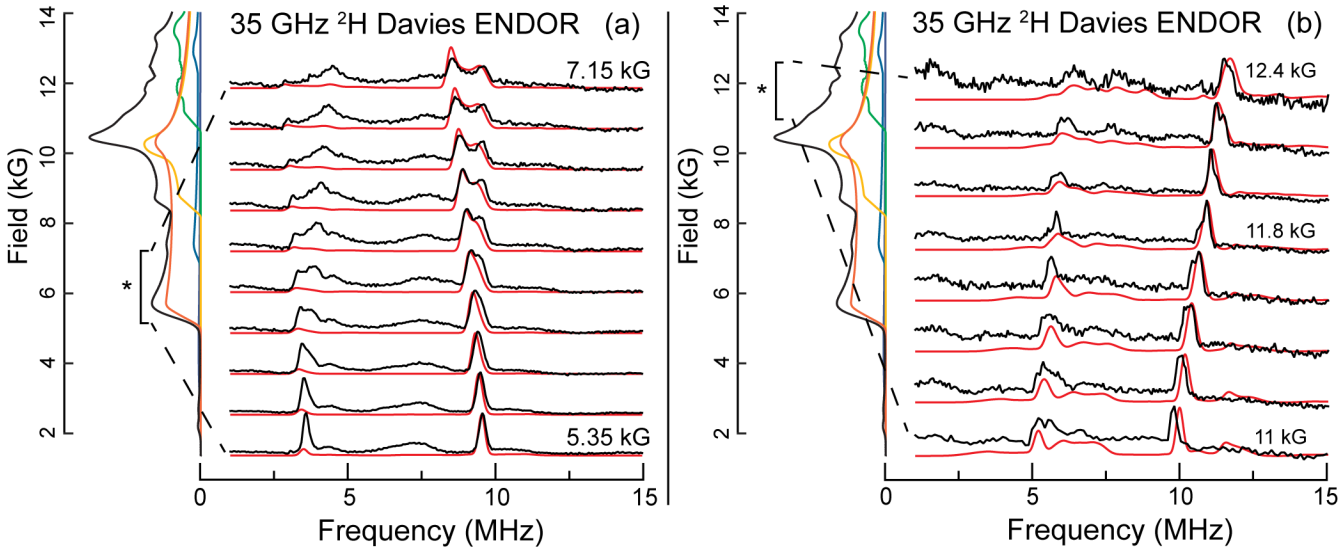

Figure 5. LEFT i.e. Figure 5(a): 2 K 35 GHz ^{2}H Davies ENDOR 2-D pattern of (^{tBu}**L**)MnD. Magnetic field values from 5.35 – 7.15 kG at 0.20 kG intervals. Black: experiment with conditions same as in Figure 4; red: EasySpin simulation with parameters of Figure S15 with $\boldsymbol{A}(^2\text{H})$ = [-5.32, -5.32, 1.0] MHz. EPR specta from Figure 3 are shown on left with the ENDOR probed region identified by an asterisk-marked bracket. Spectra normalized for clarity. RIGHT i.e. Figure 5(b): 2 K 35 GHz 2-D pattern of ^{2}H Davies(^{tBu}**L**)MnD ENDOR spectra. Field range, 11.0 – 12.4 kG, 0.2 kG intervals. Black: experiment with conditions as in Figure 4. Red, EasySpin simulations with HFI tensor of Figure 5a. *On left*: Experimental EPR spectrum from Figure 3, with EasySpin decomposition into m_s manifolds using parameters of Figure 3b**.** ENDOR-probed region highlighted by asterisk-marked bracket. Spectra scaled arbitrarily for clarity.

the axial intrinsic HFI tensor $\boldsymbol{A}(^2\text{H})$ = [–5.32, –5.32, 1.0] MHz = $a_{iso}(^2\text{H})\times\mathbf{1}$ + $\boldsymbol{T}(^2\text{H})$, yielding, $a_{iso}(^2\text{H})$ = –3.2 MHz ($a_{iso}(^1\text{H})$ = –20.9 MHz) and $\boldsymbol{T}(^2\text{H})$ = [–2.1, –2.1, 4.2] MHz ($\boldsymbol{T}(^1\text{H})$ = [−13.7, −13.7, 27.3] MHz).[54] As anticipated, the simulations show that the unique (T_3) axis lies along the unique (Z) axis of the ZFS tensor, which must in turn lie along the Mn–D bond. In addition, we again note that the pattern shows no ^{2}H quadrupole splitting, as expected.

Treating $\boldsymbol{T}(^{1,2}\text{H})$ as a dipolar interaction of the H/D nucleus with the spin on Mn gives a rough estimate of Mn–H/D distance: d(Mn-H) ≈ 1.8 Å,[72] in line with structural data and DFT calculations (see above and below). The isotropic coupling of a hydrogen nucleus to a center with spin S is proportional to the 1s-orbital spin density, ρ, through the relationship $a_{iso} = \rho a_0/2S$ where a_0= 1422.7 MHz (^{1}H) is the isotropic hyperfine constant for a single (S = 1/2) electron in a hydrogen 1s orbital.[73] This relation, and the measured $a_{iso}(^1\text{H})$ = –20.9 MHz, gives ρ = –0.073 spins for the hydride ligand of (^{tBu}**L**)MnH, with the negative sign of the spin a result of spin-polarization.

ENDOR spectroscopy at magnetic Fields in vicinity of g = 2. Figure S18 shows 35 GHz ^{1}H (a) and ^{2}H (b) Davies ENDOR spectra collected at 11.8 kG and 2 K for both (^{tBu}**L**)MnH and (^{tBu}**L**)MnD. Two distinctive ^{1}H peaks for (^{tBu}**L**)MnH in Figure S18a (red trace) at 37.8 MHz and 70.8 MHz are observed; these form a ^{1}H hydride doublet, as it matches the ^{2}H doublet observed for (^{tBu}**L**)MnD (Figure S18b, black trace) at frequencies 5.8 MHz and 10.9 MHz upon accounting for the difference in H/D nuclear g-values. The Mn–D ^{2}H doublet at 11.8 kG is centered on 8.35 MHz and split by an observed hyperfine coupling of A' = –5.1 MHz. In particular, the doublet splittings in Figures 4 and S18 correspond well with the 'perpendicular' components of the deuteron hyperfine tensor determined above, $A(^2\text{H})_{x,y}$ = –5.32 MHz, as expected for a 'powder-like' ENDOR pattern for a hyperfine tensor with $|A_\perp| >> A_\parallel \sim 0$. Figure 5b shows the 2-D ENDOR pattern of ^{2}H spectra for (^{tBu}**L**)MnD from 11.0 – 12.4 kG. In this range the contribution of the –1/2 → +1/2 transition to the EPR spectrum is emphasized (Figure 3b), and the ENDOR spectrum shows strong, well-defined signals from this manifold; signals from the other, Boltzmann depopulated, manifolds are very weak and broad because of the poor orientation selection. The 'field-evolution' of the –1/2 → +1/2 ^{2}H doublet in Figure 5b is well reproduced by EasySpin simulations using the spin-Hamiltonian hyperfine tensor given above. The simulation, which is the sum of ENDOR responses from all orientations and transitions that contribute to the EPR spectrum

at the given magnetic field, corroborates that observed well-defined ENDOR peaks are indeed ^{2}H doublets associated with the –1/2 → +1/2 manifold, while signals from other manifolds are broadened so that they are indeed indistinguishable. The center frequency of the doublet seen at the edge of the EPR spectrum, 7.5 MHz (at 11 kG) is only slightly shifted from the ^{2}H Larmor frequency $\nu_N(^2H)$ = 7.2 MHz and increases with field along with the Larmor frequency (Figure 5b), which indicates that the doublet is associated with the *nominally* –1/2 → +1/2 electron-spin transition (see SI). The overlaid EasySpin simulations (Figure 5b) show this pattern is likewise well-replicated using the hyperfine tensor determined by simulating the low-field 2D pattern of Figure 5a.

Calculations

To provide further electronic structure insights, (^{tBu}**L**)MnI and (^{tBu}**L**)MnH were subjected to computational analysis; tabulated spin-Hamiltonian parameters are presented in Table 1, along with the experimentally-determined values for comparison (details are provided in the SI). The computed *g*-tensors for (^{tBu}**L**)MnI and (^{tBu}**L**)MnH exhibit little anisotropy, as expected for high spin d^5 centers. The predicted ZFS parameters are in reasonable agreement with experiment for (^{tBu}**L**)MnH, and the calculated ^{1}H hyperfine coupling tensor, both isotropic and anisotropic components and spin density (ρ = –0.071) for the terminal hydride ligand of (^{tBu}**L**)MnH are in excellent agreement with those determined by ENDOR spectroscopy.

The experimental ZFS parameters for (^{tBu}**L**)MnI are not as well reproduced; for example, the absolute magnitude of *D* for (^{tBu}**L**)MnI is about four times larger than the value given by the EPR simulation. Calculated values of $|D|$ for Mn^{2+} complexes including heavy-element ligand(s) (e.g. I) can exhibit poor accuracy, presumably due to the approximate treatment of spin orbit coupling under a scalar-relativistic Hamiltonian (see SI for further discussion).[66] Nevertheless, the experimental trend is reproduced—*i.e.*, (^{tBu}**L**)MnI exhibits substantially higher *D*, and much smaller rhombicity, *E*/*D*, compared to (^{tBu}**L**)MnH. The results of this method accords well with our previous computational results on complexes of this ligand class,[55] which demonstrated that spin densities computed at the TPSS0 level approximate those computed at the CASSCF level. A more consistent treatment of the ZFS would likely require a similar multi-reference ansatz to properly capture the effects of spin-orbit coupling.

Table 1. Collected experimental and calculated spectroscopic parameters for (^{tBu}**L**)MnI and (^{tBu}**L**)MnH.

Parameter	(^{tBu}**L**)MnI		(^{tBu}**L**)MnH	
	Expt.	*DFT*	*Expt.*	*DFT*
g	2.0[a]	[2.002, 2.009, 2.011]	2.0[a]	[2.001, 2.002, 2.002]
***D* (MHz; cm^{-1})**	24,000; 0.83	105,000; 3.5	7,600; 0.25	5,850; 0.20
E*/*D	0.03	0.05	0.15	0.11
***A*(^{55}Mn) (MHz)**	−250[a]	− [88.9, 92.0, 92.9]	−250[a]	− [167, 176, 190]
***A*(^{1}H) (MHz)**	–	–	[−34.6, −34.6, 6.5]	[−34.2, −34.0, 7.4]

[a]Parameter assumed and not refined in EPR simulations.

DISCUSSION

The studies presented above provide the first characterization of a high-spin (S = 5/2), d^5 metal hydride. Given the good possibility that hydride-bound FeMoco intermediates feature locally d^5 Fe^{3+}–H sites, our work provides important context for the continued structural and electronic characterization of such catalytically relevant states. EPR/ENDOR studies of (^{tBu}**L**)MnH/D reveal the bound hydride/deuteride to be, as expected, strongly coupled to the Mn^{2+} center (a_{iso}(^{1}H) = –20.9 MHz). DFT calculations are in excellent agreement with the spectroscopic data obtained for (^{tBu}**L**)MnH/D, thus serving to bolster our EPR simulations, which depend on parameters not fully resolved experimentally. In line with all terminal hydride complexes for which such data are available, the anisotropic component of the Mn–H/D hyperfine tensor for (^{tBu}**L**)MnH/D exhibits roughly axial symmetry.[18-19, 74] By contrast, this further cements the assignment of E_4(4H), which features a rhombic hyperfine-coupling tensor, as containing a Fe–(μ_2-H)–Fe unit, as opposed to a terminally bound hydrido ligand(s).[10] We note, however, that under catalytically relevant conditions these hydrides are likely to be labile, and thus able to change their bonding, and even migrate between different Fe sites within the cluster. Consequently, a terminal hydride(s) of Fe forming prior to reductive elimination of H_2, as suggested by us elsewhere, may prove mechanistically important.[7]

In terms of absolute magnitude, the ^{1}H/^{2}H hyperfine interactions observed for (^{tBu}**L**)MnH/D are reasonably similar to those unambiguously determined for other half-integer

spin, terminal metal hydrides, irrespective of metal.[18-19, 74-75] Interestingly, however, the value of $a_{iso}(^1H)$ determined for (^{tBu}**L**)MnH appears to be considerably lower than that estimated for low-spin (S = 1/2) $[(dmpe)_2MnH(L)]^+$ complexes (~85 MHz; $|\rho| \approx 0.06$).[54] However, we note that the estimate of the ^1H hyperfine couplings from analysis of the EPR spectrum of the latter was compromised by the presence of extensive ^{31}P hyperfine splittings and broadened lines, and so not determined with precision; $a_{iso}(^1H)$ for these molecules could be as low as ~40 MHz, which would be more usual for low-spin hydrides.[75] Notably, (^{tBu}**L**)MnH exhibits substantially more spin density on the hydrido ligand ($|\rho|$ = 0.073; see above) than any other synthetic metal hydride for which $a_{iso}(^1H)$ has been determined with reasonable accuracy. For example, the intermediate spin (S = 3/2) $[NacNacFe^+H]^-$ features $|\rho|$ = 0.04,[19] and $|\rho| < 0.03$ is typical.[16, 18-21, 74-75] Direct comparison of the spin densities for mononuclear and polynuclear systems, including FeMoco, requires a knowledge of the spin-projection factors of the metal ions within the spin-coupled clusters. The analysis of the hyperfine tensors of the bridging Fe-H-Fe hydrides of the $E_4(4H)$ nitrogenase intermediate yields good estimates for the ratios of the spin-projection factors for the anchor Fe ions,[11] but not their absolute magnitudes.

CONCLUSION

Through use of a sufficiently sterically demanding and σ-donating heteroscorpionate supporting ligand we have isolated a complex with a terminal hydride bound to a high-spin (S = 5/2) Mn, (^{tBu}**L**)MnH. EPR and ENDOR analysis reveal an exceptional spin density on the Mn-bound hydride ligand, which is well-corroborated by DFT calculations. Given hydride-bound FeMoco intermediates are expected to feature locally high-spin Fe^{3+}–H sites, and the isoelectronic relationship between Mn^{2+} and Fe^{3+}, our results will further inform our understanding of such biological clusters. Future work will, quite naturally, aim to extend our Mn chemistry to Fe. We are curious to assess the extent to which the hydride chemistries of these metals substantially agree, and where they deviate, and the implications of these results for nitrogenase enzymes.

ACKNOWLEDGEMENTS

N.B.T. acknowledges support from U.S. DOE, Office of Science, Office of Basic Energy Sciences through Argonne National Laboratory under contract no. DE-AC02-06CH11357.

ASSOCIATED CONTENT

Supporting Information Available:

Spectroscopic data, additional figures and discussion and coordinates for all calculated structures. This information is available free of charge at the website: http://pubs.acs.org.

Crystallographic information files (.cifs) for complexes (^{tBu}**L**)MnI and (^{tBu}**L**)MnH have been uploaded to the CCDC under deposition numbers 2337917 and 2337918.

REFERENCES

(1) Norton, J. R.; Sowa, J., Introduction: Metal Hydrides. *Chem. Rev.* **2016**, *116* (15), 8315-8317.
(2) Crabtree, R. H., The organometallic chemistry of the transition metals. 7th ed.; Wiley: Hoboken, N.J., 2019; pp 80–83.
(3) Can, M.; Armstrong, F. A.; Ragsdale, S. W., Structure, Function, and Mechanism of the Nickel Metalloenzymes, Co Dehydrogenase, and Acetyl-Coa Synthase. *Chem. Rev.* **2014**, *114* (8), 4149-4174.
(4) Lubitz, W.; Ogata, H.; Rudiger, O.; Reijerse, E., Hydrogenases. *Chem. Rev.* **2014**, *114* (8), 4081-4148.
(5) Hoffman, B. M.; Lukoyanov, D.; Yang, Z. Y.; Dean, D. R.; Seefeldt, L. C., Mechanism of Nitrogen Fixation by Nitrogenase: The Next Stage. *Chem. Rev.* **2014**, *114* (8), 4041-62.
(6) Schilter, D.; Camara, J. M.; Huynh, M. T.; Hammes-Schiffer, S.; Rauchfuss, T. B., Hydrogenase Enzymes and Their Synthetic Models: The Role of Metal Hydrides. *Chem. Rev.* **2016**, *116* (15), 8693-8749.
(7) Seefeldt, L. C.; Yang, Z. Y.; Lukoyanov, D. A.; Harris, D. F.; Dean, D. R.; Raugei, S.; Hoffman, B. M., Reduction of Substrates by Nitrogenases. *Chem. Rev.* **2020**, *120* (12), 5082-5106.
(8) Canfield, D. E.; Glazer, A. N.; Falkowski, P. G., The Evolution and Future of Earth's Nitrogen Cycle. *Science* **2010**, *330* (6001), 192-196.
(9) Erisman, J. W.; Sutton, M. A.; Galloway, J.; Klimont, Z.; Winiwarter, W., How a Century of Ammonia Synthesis Changed the World. *Nat Geosci* **2008**, *1* (10), 636-639.
(10) Hoeke, V.; Tociu, L.; Case, D. A.; Seefeldt, L. C.; Raugei, S.; Hoffman, B. M., High-Resolution Endor Spectroscopy Combined with Quantum Chemical Calculations Reveals the Structure of Nitrogenase Janus Intermediate E_4(4H) (Vol 141, Pg 11984, 2019). *J. Am. Chem. Soc.* **2019**, *141* (50), 19950-19950.
(11) Igarashi, R. Y.; Laryukhin, M.; Dos Santos, P. C.; Lee, H. I.; Dean, D. R.; Seefeldt, L. C.; Hoffman, B. M., Trapping H- Bound to the Nitrogenase Femo-Cofactor Active Site During H-2 Evolution: Characterization by Endor Spectroscopy. *J. Am. Chem. Soc.* **2005**, *127* (17), 6231-6241.
(12) Lukoyanov, D.; Khadka, N.; Yang, Z. Y.; Dean, D. R.; Seefeldt, L. C.; Hoffman, B. M., Reductive Elimination of H2 Activates Nitrogenase to Reduce the N≡N Triple Bond: Characterization of the E4(4H) Janus Intermediate in Wild-Type Enzyme. *J Am Chem Soc* **2016**, *138* (33), 10674-83.

(13) Lukoyanov, D.; Yang, Z. Y.; Dean, D. R.; Seefeldt, L. C.; Hoffman, B. M., Is Mo Involved in Hydride Binding by the Four-Electron Reduced (E-4) Intermediate of the Nitrogenase Mofe Protein? *J. Am. Chem. Soc.* **2010**, *132* (8), 2526-+.
(14) Lukoyanov, D.; Khadka, N.; Yang, Z. Y.; Dean, D. R.; Seefeldt, L. C.; Hoffman, B. M., Reversible Photoinduced Reductive Elimination of H

from the Nitrogenase Dihydride State, the E

(4h) Janus Intermediate. *J. Am. Chem. Soc.* **2016**, *138* (4), 1320-1327.
(15) Lukoyanov, D. A.; Khadka, N.; Yang, Z. Y.; Dean, D. R.; Seefeldt, L. C.; Hoffman, B. M., Hydride Conformers of the Nitrogenase Femo-Cofactor Two-Electron Reduced State E

(2h), Assigned Using Cryogenic Intra Electron Paramagnetic Resonance Cavity Photolysis. *Inorg. Chem.* **2018**, *57* (12), 6847-6852.
(16) Keizer, P. N.; Krusic, P. J.; Morton, J. R.; Preston, K. F., Thiolato-Bridged and Selenato-Bridged Dinuclear Iron Carbonyl Radicals. *J. Am. Chem. Soc.* **1991**, *113* (14), 5454-5456.
(17) Lees, N. S.; McNaughton, R. L.; Gregory, W. V.; Holland, P. L.; Hoffman, B. M., Endor Characterization of a Synthetic Diiron Hydrazido Complex as a Model for Nitrogenase Intermediates. *J. Am. Chem. Soc.* **2008**, *130* (2), 546-555.
(18) Kinney, R. A.; Hetterscheid, D. G. H.; Hanna, B. S.; Schrock, R. R.; Hoffman, B. M., Formation of {[HiptnN]Mo(Iii)H} by Heterolytic Cleavage of H as Established by Epr and Endor Spectroscopy. *Inorg. Chem.* **2010**, *49* (2), 704-713.

Modeling the signatures of hydrides in metalloenzymes: ENDOR analysis of a Di-iron Fe(mu-NH)(mu-H)Fe core R. A. Kinney, C. T. Saouma, J. C. Peters and B. M. Hoffman J Am Chem Soc 2012 Vol. 134 Issue 30 Pages 12637-47

Accession Number: 22823933 PMCID: 3433054 DOI: 10.1021/ja303739ghttp://www.ncbi.nlm.nih.gov/pubmed/22823933

(19) Chiang, K. P.; Scarborough, C. C.; Horitani, M.; Lees, N. S.; Ding, K. Y.; Dugan, T. R.; Brennessel, W. W.; Bill, E.; Hoffman, B. M.; Holland, P. L., Characterization of the Fe?H Bond in a Three-Coordinate Terminal Hydride Complex of Iron(I). *Angew. Chem. Int. Ed.* **2012**, *51* (15), 3658-3662.
(20) Kinney, R. A.; Saouma, C. T.; Peters, J. C.; Hoffman, B. M., Modeling the Signatures of Hydrides in Metalloenzymes: Endor Analysis of a Di-Iron Fe(Mu-Nh)(Mu-H)Fe Core. *J. Am. Chem. Soc.* **2012**, *134* (30), 12637-12647.
(21) Arnett, C. H.; Bogacz, I.; Chatterjee, R.; Yano, J.; Oyala, P. H.; Agapie, T., Mixed-Valent Diiron M-Carbyne, M-Hydride Complexes: Implications for Nitrogenase. *J. Am. Chem. Soc.* **2020**, *142* (44), 18795-18813.
(22) Jewson, J. D.; Liable-Sands, L. M.; Yap, G. P. A.; Rheingold, A. L.; Theopold, K. H., Paramagnetic Alkyl, Hydride, and Alkene Complexes of the Tp(T-Bu,Me)Co Moiety. *Organometallics* **1999**, *18* (3), 300-305.
(23) Smith, J. M.; Lachicotte, R. J.; Holland, P. L., N=N Bond Cleavage by a Low-Coordinate Iron(Ii) Hydride Complex. *J. Am. Chem. Soc.* **2003**, *125* (51), 15752-15753.
(24) Sadique, A. R.; Gregory, E. A.; Brennessel, W. W.; Holland, P. L., Mechanistic Insight into N=N Cleavage by a Low-Coordinate Iron(Ii) Hydride Complex. *J. Am. Chem. Soc.* **2007**, *129* (26), 8112-8121.
(25) Yu, Y.; Sadique, A. R.; Smith, J. M.; Dugan, T. R.; Cowley, R. E.; Brennessel, W. W.; Flaschenriem, C. J.; Bill, E.; Cundari, T. R.; Holland, P. L., The Reactivity Patterns of Low-Coordinate Iron-Hydride Complexes. *J. Am. Chem. Soc.* **2008**, *130* (20), 6624-6638.

(26) Ding, K. Y.; Brennessel, W. W.; Holland, P. L., Three-Coordinate and Four-Coordinate Cobalt Hydride Complexes That React with Dinitrogen. *J. Am. Chem. Soc.* **2009**, *131* (31), 10804-+.
(27) Blair, V. L.; Carrella, L. M.; Clegg, W.; Klett, J.; Mulvey, R. E.; Rentschler, E.; Russo, L., Structural and Magnetic Insights into the Trinuclear Ferrocenophane and Unexpected Hydrido Inverse Crown Products of Alkali-Metal-Mediated Manganation(Ii) of Ferrocene. *Chem. - Eur. J.* **2009**, *15* (4), 856-863.
(28) Chomitz, W. A.; Arnold, J., Synthesis and Characterization of Manganese and Iron Complexes Supported by Multidentate [N2p2] Ligands. *Dalton Trans.* **2009**, (10), 1714-1720.
(29) Yao, S. L.; Xiong, Y.; Driess, M., Facile Metalation of Silicon and Germanium Analogues of Thiocarboxylic Acids with a Manganese(Ii) Hydride Precursor. *Chem. - Eur. J.* **2012**, *18* (36), 11356-11361.
(30) Lee, Y.; Anderton, K. J.; Sloane, F. T.; Ermert, D. M.; Abboud, K. A.; Garcia-Serres, R.; Murray, L. J., Reactivity of Hydride Bridges in High-Spin [3m-3(Mu-H)] Clusters (M = Fe-Ii, Co-Ii). *J. Am. Chem. Soc.* **2015**, *137* (33), 10610-10617.
(31) Arnet, N. A.; Dugan, T. R.; Menges, F. S.; Mercado, B. Q.; Brennessel, W. W.; Bill, E.; Johnson, M. A.; Holland, P. L., Synthesis, Characterization, and Nitrogenase-Relevant Reactions of an Iron Sulfide Complex with a Bridging Hydride. *J. Am. Chem. Soc.* **2015**, *137* (41), 13220-13223.
(32) Gehring, H.; Metzinger, R.; Braun, B.; Herwig, C.; Harder, S.; Ray, K.; Limberg, C., An Iron(Ii) Hydride Complex of a Ligand with Two Adjacent B-Diketiminate Binding Sites and Its Reactivity. *Dalton Trans.* **2016**, *45* (7), 2989-2996.
(33) Bellows, S. M.; Arnet, N. A.; Gurubasavaraj, P. M.; Brennessel, W. W.; Bilks, E.; Cundari, T. R.; Holland, P. L., The Mechanism of N-N Double Bond Cleavage by an Iron(Ii) Hydride Complex. *J. Am. Chem. Soc.* **2016**, *138* (37), 12112-12123.
(34) Fohlmeister, L.; Jones, C., Stabilisation of Carbonyl Free Amidinato-Manganese(Ii) Hydride Complexes: "Masked" Sources of Manganese(I) in Organometallic Synthesis. *Dalton Trans.* **2016**, *45* (4), 1436-1442.
(35) Anderton, K. J.; Ermert, D. M.; Quintero, P. A.; Turvey, M. W.; Fataftah, M. S.; Abboud, K. A.; Meisel, M. W.; Cizmar, E.; Murray, L. J., Correlating Bridging Ligand with Properties of Ligand-Templated [(Mn3x3)-X-Ii](3+) Clusters (X = Br-, Cl-, H-, Meo-). *Inorg. Chem.* **2017**, *56* (19), 12012-12022.
(36) Anderton, K. J.; Knight, B. J.; Rheingold, A. L.; Abboud, K. A.; Garcia-Serres, R.; Murray, L. J., Reactivity of Hydride Bridges in a High-Spin [Fe-3(Mu-H)(3)](3+) Cluster: Reversible H-2/Co Exchange and Fe-H/B-F Bond Metathesis. *Chem Sci* **2017**, *8* (5), 4123-4129.
(37) MacLeod, K. C.; Lewis, R. A.; DeRosha, D. E.; Mercado, B. Q.; Holland, P. L., C-H and C-N Activation at Redox-Active Pyridine Complexes of Iron. *Angew. Chem. Int. Ed.* **2017**, *56* (4), 1069-1072.
(38) Sekiguchi, Y.; Kuriyama, S.; Eizawa, A.; Arashiba, K.; Nakajima, K.; Nishibayashi, Y., Synthesis and Reactivity of Iron-Dinitrogen Complexes Bearing Anionic Methyl- and Phenyl-Substituted Pyrrole-Based Pnp-Type Pincer Ligands toward Catalytic Nitrogen Fixation. *Chem. Commun.* **2017**, *53* (88), 12040-12043.
(39) Hein, N. M.; Pick, F. S.; Fryzuk, M. D., Synthesis and Reactivity of a Low-Coordinate Iron(Ii) Hydride Complex: Applications in Catalytic Hydrodefluorination. *Inorg. Chem.* **2017**, *56* (23), 14513-14523.
(40) Ott, J. C.; Wadepohl, H.; Enders, M.; Gade, L. H., Taking Solution Proton Nmr to Its Extreme: Prediction and Detection of a Hydride Resonance in an Intermediate-Spin Iron Complex. *J. Am. Chem. Soc.* **2018**, *140* (50), 17413-17417.
(41) Hickey, A. K.; Greer, S. M.; Valdez-Moreira, J. A.; Lutz, S. A.; Pink, M.; DeGayner, J. A.; Harris, T. D.; Hill, S.; Telser, J.; Smith, J. M., A Dimeric Hydride-Bridged Complex with Geometrically Distinct Iron Centers Giving Rise to an S=3 Ground State. *J. Am. Chem. Soc.* **2019**, *141* (30), 11970-11975.
(42) Gasperini, D.; King, A. K.; Coles, N. T.; Mahon, M. F.; Webster, R. L., Seeking Heteroatom-Rich Compounds: Synthetic and Mechanistic Studies into Iron Catalyzed Dehydrocoupling of Silanes. *Acs Catal* **2020**, *10* (11), 6102-6112.

(43) McWilliams, S. F.; Broere, D. L. J.; Halliday, C. J. V.; Bhutto, S. M.; Mercado, B. Q.; Holland, P. L., Coupling Dinitrogen and Hydrocarbons through Aryl Migration. *Nature* **2020**, *584* (7820), 221-+.
(44) Handford, R. C.; Nguyen, T. T.; Teat, S. J.; Britt, R. D.; Tilley, T. D., Direct Transformation of Sih4 to a Molecular L(H)2co=Si=Co(H)2l Silicide Complex. *J. Am. Chem. Soc.* **2023**.
(45) McWilliams, S. F.; Mercado, B. Q.; MacLeod, K. C.; Fataftah, M. S.; Tarrago, M.; Wang, X. P.; Bill, E.; Ye, S. F.; Holland, P. L., Dynamic Effects on Ligand Field from Rapid Hydride Motion in an Iron(Ii) Dimer with an S=3 Ground State. *Chem Sci* **2023**, *14* (9), 2303-2312.
(46) Van Stappen, C.; Decamps, L.; Cutsail, G. E.; Bjornsson, R.; Henthorn, J. T.; Birrell, J. A.; DeBeer, S., The Spectroscopy of Nitrogenases. *Chem. Rev.* **2020**, *120* (12), 5005-5081.
(47) Beinert, H.; Holm, R. H.; Munck, E., Iron-Sulfur Clusters: Nature's Modular, Multipurpose Structures. *Science* **1997**, *277* (5326), 653-659.
(48) Ye, M.; Thompson, N. B.; Brown, A. C.; Suess, D. L. M., A Synthetic Model of Enzymatic [Fe4s4]-Alkyl Intermediates. *J Am Chem Soc* **2019**, *141* (34), 13330-13335.
(49) McSkimming, A.; Sridharan, A.; Thompson, N. B.; Muller, P.; Suess, D. L. M., An [Fe4s4](3+)-Alkyl Cluster Stabilized by an Expanded Scorpionate Ligand. *J. Am. Chem. Soc.* **2020**, *142* (33), 14314-14323.
(50) Sridharan, A.; Brown, A. C.; Suess, D. L. M., A Terminal Imido Complex of an Iron-Sulfur Cluster. *Angew. Chem. Int. Ed.* **2021**, *60* (23), 12802-12806.
(51) Brown, A. C.; Thompson, N. B.; Suess, D. L. M., Evidence for Low-Valent Electronic Configurations in Iron-Sulfur Clusters. *J. Am. Chem. Soc.* **2022**, *144* (20), 9066-9073.
(52) Kim, Y.; Sridharan, A.; Suess, D. L. M., The Elusive Mononitrosylated [Fe4s4] Cluster in Three Redox States. *Angew. Chem. Int. Ed.* **2022**, *61* (47).
(53) Maekawa, M.; Römelt, M.; Daniliuc, C. G.; Jones, P. G.; White, P. S.; Neese, F.; Walter, M. D., Reactivity Studies on [Cp'Mnx(Thf)]

: Manganese Amide and Polyhydride Synthesis. *Chem Sci* **2012**, *3* (10), 2972-2979.
(54) Rennie, B. E.; Price, J. S.; Emslie, D. J. H.; Morris, R. H., Trans Ligand Determines the Stability of Paramagnetic Manganese(Ii) Hydrides of the Type Trans-[Mnh(L)(Dmpe)2]+ Where L Is Pme3, C2h4, or Co. *Inorg. Chem.* **2023**, *62* (21), 8123-8135.
(55) McSkimming, A.; Thompson, N. B., Four-Coordinate Fe N-2 and Imido Complexes Supported by a Hemilabile Nnc Heteroscorpionate Ligand. *Inorg. Chem.* **2022**, *61* (31), 12318-12326.
(56) Gu, L.; Fraker, A.; McSkimming, A., Dynamic N-2 Binding at High-Spin Co(I) Supported by N,N,C Heteroscorpionates. *Organometallics* **2023**, *42* (13), 1621-1628.
(57) Kaesz, H. D.; Saillant, R. B., Hydride Complexes of Transition-Metals. *Chem. Rev.* **1972**, *72* (3), 231-&.
(58) Stoll, S.; Schweiger, A., Easyspin, a Comprehensive Software Package for Spectral Simulation and Analysis in Epr. *J Magn Reson* **2006**, *178* (1), 42-55.
(59) Smoukov, S. K.; Telser, J.; Bernat, B. A.; Rife, C. L.; Armstrong, R. N.; Hoffman, B. M., Epr Study of Substrate Binding to the Mn(Ii) Active Site of the Bacterial Antibiotic Resistance Enzyme Fosa: A Better Way to Examine Mn(Ii). *J. Am. Chem. Soc.* **2002**, *124* (10), 2318-2326.
(60) Duboc, C.; Collomb, M. N.; Neese, F., Understanding the Zero-Field Splitting of Mononuclear Manganese(Ii) Complexes from Combined Epr Spectroscopy and Quantum Chemistry. *Appl Magn Reson* **2010**, *37* (1-4), 229-245.
(61) Sharma, A.; Gaidamakova, E. K.; Matrosova, V. Y.; Bennett, B.; Daly, M. J.; Hoffman, B. M., Responses of Mn

Speciation in

and

to Γ-Radiation by Advanced Paramagnetic Resonance Methods. *P Natl Acad Sci USA* **2013**, *110* (15), 5945-5950.
(62) Wood, R. M.; Stucker, D. M.; Jones, L. M.; Lynch, W. B.; Misra, S. K.; Freed, J. H., An Epr Study of Some Highly Distorted Tetrahedral Manganese(Ii) Complexes at High Magnetic Fields. *Inorg. Chem.* **1999**, *38* (23), 5384-5388.
(63) Girolami, G. S.; Wilkinson, G.; Galas, A. M. R.; Thorntonpett, M.; Hursthouse, M. B., Synthesis and Properties of the Divalent 1,2-Bis(Dimethylphosphino)Ethane (Dmpe) Complexes Mcl2(Dmpe)2 and Mme2(Dmpe)2 (M=Ti, V, Cr, Mn, or Fe) - X-Ray Crystal-Structures of Mcl2(Dmpe)2 (M=Ti, V, or Cr), Mnbr2(Dmpe)2, Time1.3cl0.7(Dmpe)2, and Crme2(Dmpe). *J. Chem. Soc. Dalton Trans.* **1985**, (7), 1339-1348.
(64) Mantel, C.; Baffert, C.; Romero, I.; Deronzier, A.; Pécaut, J.; Collomb, M. N.; Duboc, C., Structural Characterization and Electronic Properties Determination by High-Field and High-Frequency Epr of a Series of Five-Coordinated Mn(Ii) Complexes. *Inorg. Chem.* **2004**, *43* (20), 6455-6463.
(65) Duboc, C.; Phoeung, T.; Zein, S.; Pecaut, J.; Collomb, M. N.; Neese, F., Origin of the Zero-Field Splitting in Mononuclear Octahedral Dihalide Mn

Complexes:: An Investigation by Multifrequency High-Field Electron Paramagnetic Resonance and Density Functional Theory. *Inorg. Chem.* **2007**, *46* (12), 4905-4916.
(66) Zein, S.; Duboc, C.; Lubitz, W.; Neese, F., A Systematic Density Functional Study of the Zero-Field Splitting in Mn(Ii) Coordination Compounds. *Inorg. Chem.* **2008**, *47* (1), 134-142.
(67) Horitani, M.; Offenbacher, A. R.; Carr, C. A. M.; Yu, T.; Hoeke, V.; Cutsail, G. E.; Hammes-Schiffer, S.; Klinman, J. P.; Hoffman, B. M., C Endor Spectroscopy of Lipoxygenase-Substrate Complexes Reveals the Structural Basis for C-H Activation by Tunneling. *J. Am. Chem. Soc.* **2017**, *139* (5), 1984-1997.
(68) Sharma, A.; Whittington, C.; Jabed, M.; Hill, S. G.; Kostenko, A.; Yu, T.; Li, P. F.; Doan, P. E.; Hoffman, B. M.; Offenbacher, A. R., 13c Electron Nuclear Double Resonance Spectroscopy-Guided Molecular Dynamics Computations Reveal the Structure of the Enzyme-Substrate Complex of an Active, N-Linked Glycosylated Lipoxygenase. *Biochemistry-Us* **2023**, *62* (10), 1531-1543.
(69) Schweiger, A.; Jeschke, G., Principles of Pulse Electron Paramagnetic Resonance. Oxford University Press: Oxford, UK, 2001; pp 1-578.
(70) Doan, P. E.; Hoffman, B. M., Making Hyperfine Selection in Mims Endor Independent of Deadtime. *Chem Phys Lett* **1997**, *269* (3-4), 208-214.
(71) Astashkin, A. V.; Raitsimring, A. M., Refocused Primary Echo: A Zero Dead Time Detection of the Electron Spin Echo Envelope Modulation. *J Magn Reson* **2000**, *143* (2), 280-291.
(72) Snetsinger, P. A.; Chasteen, N. D.; Vanwilligen, H., Structural-Analysis of a Low-Spin Cyanide Adduct of Iron(Iii) Transferrin by Angle-Selected C-13 Endor Spectroscopy. *J. Am. Chem. Soc.* **1990**, *112* (22), 8155-8160.
(73) Fitzpatrick, J. A. J.; Manby, F. R.; Western, C. M., The Interpretation of Molecular Magnetic Hyperfine Interactions. *J Chem Phys* **2005**, *122* (8).
(74) Gu, N. X.; Oyala, P. H.; Peters, J. C., H-2 Evolution from a Thiolate-Bound Ni(Iii) Hydride. *J. Am. Chem. Soc.* **2020**, *142* (17), 7827-7835.
(75) Hu, Y.; Shaw, A. P.; Estes, D. P.; Norton, J. R., Transition-Metal Hydride Radical Cations. *Chem. Rev.* **2016**, *116* (15), 8427-8462.

TOC graphic:

A high-spin Mn–H: